ACS OMEGA

http://pubs.acs.org/journal/acsodf

Article

Texture and Magnetic Property of Fe-6.5 wt % Si Steel Strip with Cu-Rich Particles Modification

Di Zhang, Yingtao Su, Xingrui Yang, Huilan Sun, Zhihong Guo, Bo Wang,* Cheng Ma,* Zhongqi Dong, and Liguang Zhu

Cite This: *ACS Omega* 2023, 8, 8461−8472

Read Online

ACCESS | Metrics & More | Article Recommendations

ABSTRACT: Based on the ordered phase effectively suppressed by rapid solidification technology, the grain refinement concept using Cu is incorporated into the soft magnetic materials. Cu dosage not only could refine the grain size with an average grain size of 8.7 μm but also improve the continuity and consistency of Fe-6.5 wt % Si steel strip. It mainly attributes to the Cu-rich particles precipitating at the grain boundary, nailing the grain boundaries movement and inhibiting the grain growth, and then improving the magnetic properties and mechanical properties. The 1.5 wt % Cu sample exhibits an excellent magnetic property with the saturation magnetization of 236.54 emu/g, which mainly attributes to the strong η, λ, Goss texture formation and the band structure optimization of Si−Cu comodification. Furthermore, the mechanical properties of the steel strip are effectively improved, and the failure plastic deformation of 1.5 wt % Cu steel strip is about 11%. The rapid solidification with Cu-dosage refinement technology also has a remarkable reference on the mechanical properties and magnetic properties modification of other metal materials.

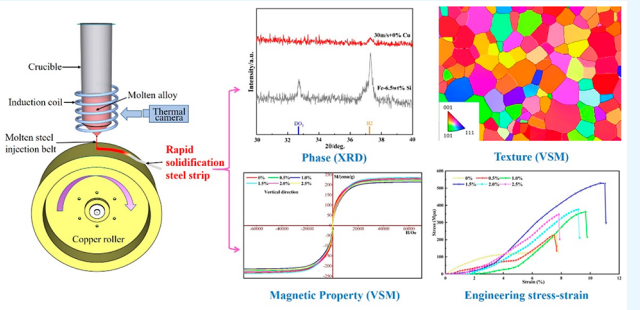

1. INTRODUCTION

As an advanced crystalline soft magnetic material, high silicon steel (Si content ≥4.5 wt %) is an important soft magnetic and functional material for electrical instruments, for instance, generators, motors, transformers, relays and other electrical instruments.[1−3] Compared with conventional Fe-3.2 wt % Si steel, Fe-6.5 wt % Si silicon steel shows better magnetic properties,[4,5] low iron loss, high permeability, good saturation magnetization, and a near zero magnetostriction coefficient. Nevertheless, as advanced functional magnetic materials, silicon steel will inevitably generate energy loss during use. The iron loss generated by silicon steel will still cause huge power consumption year-by-year, accounting for 2.8−4.9% of the global power generation.[6] Therefore, improved magnetic and mechanical properties of silicon steel have a significant impact on improving the efficiency of electrical appliances and saving energy. Increased silicon content will increase the brittleness property of silicon-containing steel, while it also could significantly improve the magnetic property. Because high-silicon content (Si content ≥4.5 wt %) steel is prone to cracks during the traditional rolling process,[1,4,7] it frequently necessitates repeated rolling heat treatment operations, resulting in high cost of high-silicon steel produced with traditional casting-rolling processes. This hot brittleness seriously hinders the development and application of Fe-6.5 wt % Si high-silicon steel.[8] The preparation of high-silicon steel materials by rapid solidification technology can effectively inhibit the formation of ordered phases (B2, DO_3)[6,9,10] and greatly improve the mechanical properties of high-silicon steel. Therefore, the rapid solidification and strip casting technology[11,12] was used in the experiment to prepare high silicon strip materials with remarkable magnetic and mechanical properties, which also has significant reference value for other functional materials.

Numerous literatures have proposed that control of silicon content,[13] inhibitor element doping,[6,14] and optimization of cooling system[15] can improve the average grain size and ordered phase transition process, thereby improving plasticity and processability.[16,17] The increase of Si content facilitates grain boundary migration, leading to the formation of large-sized grains, thereby significantly deteriorating the ductility of Si-containing steel. Grain boundary polarizing elements (Cu, Ni, Cr, Sn, Mo)[18,19] and dispersed secondary phase formation-transformation (e.g., MnS, CuS, AlN, MnSe, NbC)[13,20,21] can also suppress primary recrystallized grain growth and fixation

Received: November 23, 2022
Accepted: February 14, 2023
Published: February 24, 2023

grain boundaries.[22,23] Meanwhile, previous literatures have shown that the mechanical properties of 6.5 wt % Si electrical steel could be significantly improved with alloying technology. However, the strengthening mechanism of alloying elements on the magnetic properties of Fe-6.5 wt % Si electrical steel is not thorough enough. Many studies have shown that Ni, Ce and Al alloying elements can improve the magnetic induction of 6.5 wt % Si-containing electrical steel,[24−26] but they also increase the iron loss. In addition, other alloying elements such as Nb and Cr,[6,27] although they can improve the ductility of 6.5 wt % Si electrical steel, can degrade the magnetic properties of 6.5 wt % Si electrical steel. The effects of these alloying elements on the magnetic-mechanical properties of high silicon steels may be related to the changes in the microstructure (type and size of grains, precipitates and inclusions) and texture after alloying. At present, the research on adding Cu alloying element to steel to improve its properties is more and more extensive. For example, the Fe-22Mn-0.6C twinning-induced plasticity steel, a coherent disordered Cu-rich phase is formed by adding Cu alloying elements to improve the yield strength of ultrafine-grained (UFG) structure.[17] Some studies have also shown that Cu-rich precipitates with bcc structure can be obtained by adding Cu alloying elements to stainless steel, thus achieving good strength and plastic combination properties.[28] Some studies have shown that Cu addition to silicon steel can effectively refine the grains,[18,25,29] thereby improving the magnetic-mechanical properties of high-silicon content steel. However, there is no systematic research on Cu-rich precipitates in high-silicon steel strips, so the consistent reinforcement mechanism remains unclear due to the complex formation, transformation, and diffusion process of Cu-rich precipitates. At present, the thin strip of Fe-6.5 wt % Si steel prepared by rapid solidification technology has poor continuity, and its length is usually between 15 and 25 cm. Therefore, it is of great significance to try to add alternative elements to improve the continuity of Fe-6.5 wt % Si strip.

Therefore, in order to improve the magnetic-mechanical properties of high silicon-containing strip, Cu is added to Fe-6.5 wt % Si steel as an inhibitor, and the high silicon-containing strip is prepared in the rapid solidification technology (30 m/s). The influence mechanism of Cu addition on the magnetic-mechanical properties of high silicon steel during rapid solidification was systematically discussed. The phase transformation process, microstructure evolution, and texture characteristics of Fe-6.5 wt % Si strip with Cu addition element are also confirmed and observed. It is investigated whether there is an optimal copper dosage range for 6.5 wt % Si strip with the rapid solidification and strip casting technology to significantly improve the magnetic and mechanical properties.

2. EXPERIMENTAL SECTION

The master alloy used for rapid solidification is prepared from raw materials of iron, silicon, and copper chunks (>99.9%). Alloy raw materials with different Cu contents (0−2.5 wt %) were repeatedly smelted (6−8 times) in a high-vacuum arc melting furnace to prepare alloy ingots. After that, the master alloy was remelted in a quartz crucible of a high-vacuum single-roll belt spinning furnace using a high-efficiency electromagnetic heating device. Before preparing the steel strip by rapid solidification, the vacuum degree of the melting chamber of the strip furnace was controlled below 6.0×10^{-4} Pa, and then Ar (99.99%) was injected to make the vacuum degree of the melting chamber −0.07 to −0.04 MPa. The molten Fe−Si master alloys with different Cu dosages were injected onto a rotating copper roll using high-purity Ar and spun into a strip (Figure 1). The wheel speed of the copper wheel was precisely

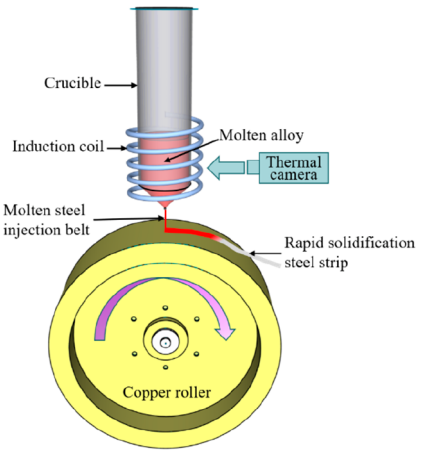

Figure 1. Schematic diagram of rapid solidification single roll spinning.

controlled and monitored by motor control system. A thermal camera was set up to record the ribbon surface temperature through a sapphire window during the melt spinning process. Multiple frames were used to acquire the average cooling rate for wheel speed. The spouted molten master alloy forms a high-silicon steel strip with a cooling rate of 8×10^5 K/s (30 m/s).

The thermal evolution of the Fe−Si−Cu steel strip samples was conducted using thermogravimetric analysis and differential scanning calorimetry (TG-DSC, Mettler TGA/DSC3+) equipment from room temperature to 1000 °C with a heating rate of 5 °C/min. The grain morphology and the texture of Fe−Si−Cu steel strip sample were characterized by electron back-scattered diffraction (EBSD, Oxford SYMMETRY), and data analysis was postprocessed with HKL-Channel 5 software to characterize. Considering typical orientations that are developed in silicon steel (Figure 2), $\varphi_2 = 0°$ and $\varphi_2 = 45°$ orientation distribution function (ODF) sections were used in this study. The hysteresis loops of the steel strip samples were confirmed by vibrating sample magnetometer (VSM, MPMS-VSM, and MPMS-XL) devices at 25 °C. Vickers hardness and engineering stress−strain curves of the samples were obtained with HVS-30 and Instron-3344 devices.

Modeling by density functional theory (DFT) and simulation calculations for phase stability and magnetic properties. The compositions are assumed to be Fe-12 atom % Si (equivalent to 6.4 wt % Si) and Fe-12 atom % Si-1 atom % Cu (equivalent to 6.4 wt % Si, 1.3 wt % Cu). The exchange-correlation energy was calculated using the generalized gradient approximation and the projector augmented wave method in the Vienna Ab-Initio Simulation Package, and the plane wave energy cutoff was 350 eV. A 2 × 2 × 2 supercell of 16 atoms was used for the modeling with the lattice parameters of $a = b = c = 5.7328$ Å of the bcc lattice. Fe−Si alloys (VCA = 0.88, 0.12) and Fe−Si−Cu alloys (VCA = 0.87, 0.12, 0.01) were simulated by virtual crystal approximation. A Γ-centered grid of 4 × 4 × 4 k-points was used for Brillouin zone sampling, and a tetrahedron method with Bloch corrections was used for the k-point integration.

https://doi.org/10.1021/acsomega.2c07510
ACS Omega 2023, 8, 8461−8472

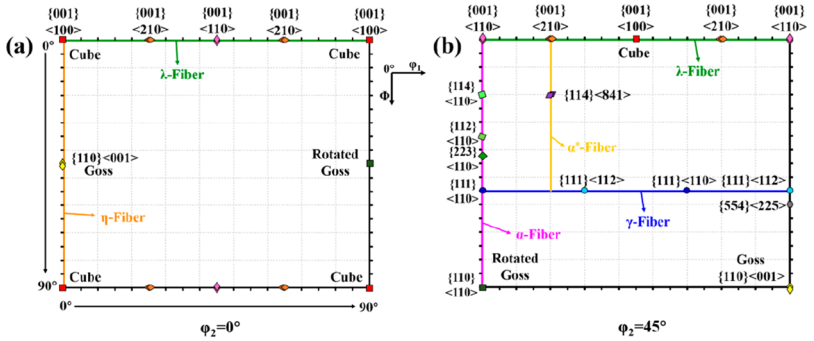

Figure 2. Typical texture components of silicon steel in (a) φ_2 = 0° and (b) φ_2 = 45° ODF sections.

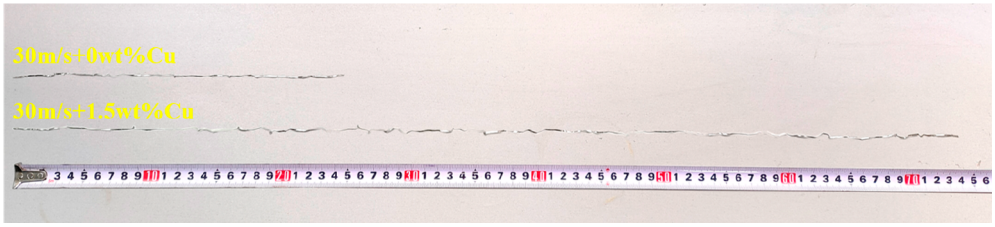

Figure 3. Photos of the Fe-6.5 wt % Si steel strip at 30 m/s.

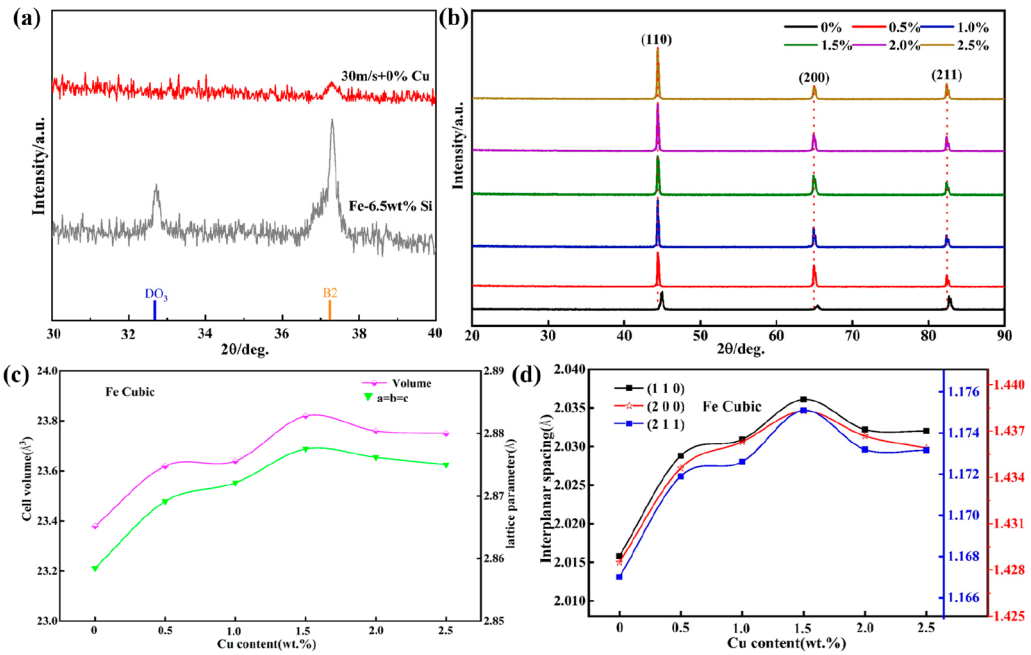

Figure 4. (a) XRD patterns of Fe-6.5 wt % Si master-alloy sample and steel strip sample for 30°−40°. (b) XRD patterns of Fe-6.5 wt % Si steel strip with 0−2.5 wt % Cu dosage. (c) Cell volume and lattice of parameters Fe. (d) Interplanar spacing of Fe.

3. RESULTS AND DISCUSSION

3.1. Sample Morphologies. The cooling rate of high silicon steel strip prepared by rapid solidification technology is 8 × 10^5 K/s (30 m/s). The steel strip samples with Cu addition have a significant difference in length compared to those without Cu addition, as shown in Figure 3. The steel strip length without Cu addition is about 25 (±5) cm, while the length of the 1.5 wt % Cu steel strip samples is about 75 (±5) cm. The addition of Cu greatly improves the continuity of the steel strip, and the roughness of the free surface and the roller surface of the steel strip is obviously different, which the most important cause of this is the different solidification environment and conditions on both sides of the steel strip during the stripping process. The molten master alloy flows through the nozzle under the pressure of high-pressure gas come into contact with the cooling copper roll, and the roll surface formed by the restraint of the cooling copper roll is relatively flat. Since the free surface is far away from the surface of the copper roll, its cooling rate is less than that of the roller surface, and the free surface forms macroscopic undulations due to it is not restrained by the copper roll during the rapid solidification and is impacted by the external high-speed airflow. There is no significant difference in the thickness and width of the thin strip samples. The average width and

https://doi.org/10.1021/acsomega.2c07510
ACS Omega 2023, 8, 8461−8472

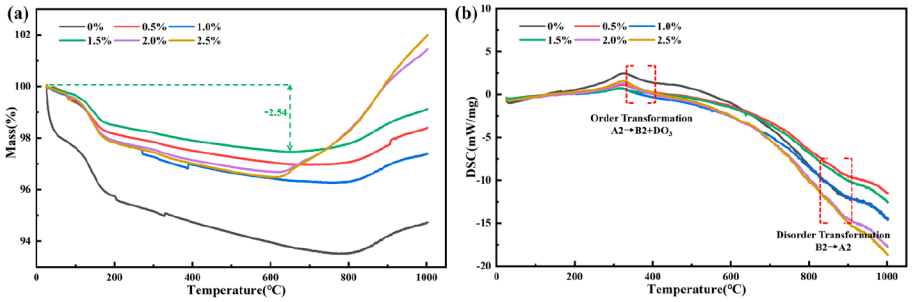

Figure 5. (a) TG curves of Fe-6.5 wt % Si steel strip with 0−2.5 wt % Cu dosage. (b) DSC curves of Fe-6.5 wt % Si steel strip with 0−2.5 wt % Cu dosage.

thickness of the sample reach 1.8 (±0.2) mm and 16.5 (±1.2) μm.

3.2. Phase Formation and Transition Process. The degree of undercooling and temperature gradient during solidification undoubtedly determine the dynamics and thermodynamics process of nucleation, crystal growth, and crystal structure transformation. Different Cu dosage also significantly affects the grain nucleation and growth of high-silicon steels during rapid solidification. Meanwhile, different Cu dosage (0 wt %-2.5 wt %) also has a great influence on the stability of crystal structure and the process of mineral formation/transition, as shown in Figure 4. In addition, the lattice parameters and space group of the cell with different Cu dosage compared with the standard phase were calculated corresponding to the XRD results.

Figure 4a shows that the B2 ordered phase and the DO_3 ordered phase clearly exist in the high-silicon steel base metal. The high-silicon steel strip prepared by rapid solidification technology at a wheel speed of 30 m/s can effectively suppress the ordered phase, in which the DO_3 ordered phase is completely suppressed and the B2 ordered phase is basically suppressed.[30,31] This is mainly due to the increase of cooling rate in the rapid solidification process, which makes the disordered phase A2 better than the ordered phase B2, and DO_3 phase precipitates and increases rapidly, thus inhibiting the ordered phase. On this basis, different Cu contents were added to the high-silicon steel to further improve the magnetic and mechanical properties of the high-silicon steel strip. Figure 4b shows the XRD patterns of high-silicon steel strip with different Cu dosage. As shown in Figure 4b,d, the comparison of steel strips with different Cu dosage at 30 m/s shows that the diffraction angle (2θ) decreases slightly (44.84° → 43.68°, 65.32° → 64.84°, and 82.66° → 82.36°). According to the Bragg eq ($2d \sin \theta = n\lambda$), it can be calculated that the interplanar spacing of the strong diffraction peaks gradually increases with the increase of Cu dosage.

The Fe crystal belongs to the cubic structure and $Im\bar{3}m$ (229) group space, while the crystal orientations are (1 1 0), (2 0 0), and (2 1 1). We also calculated the cell parameters of the steel strip based on the XRD data. Figure 4c shows the lattice constants and unit cell volumes corresponding to Fe of steel strips with different Cu dosage. Figure 4d exhibits the variation curve of the interplanar spacing of the strong diffraction peaks with different Cu dosage. Numerous factors contribute to the production and transformation of phase,[31] which then enhance their mechanical, magnetic, and chemical stability. These factors include atomic vibration/substitution processes as well as self-adjustment of crystal structure. When the Cu dosage is <1.5 wt %, Figure 4c,d demonstrates that raising the Cu dosage will gradually increase the lattice parameters (a, b, and c), cell volume, and the interplanar spacing of Fe. However, if the Cu dosage was increased beyond 1.5 wt %, the cell parameters would exhibit the reverse trend. This phenomenon is because the alloy reaches the solid solution limit near the Cu content of 1.5 wt %. Increasing Cu addition beyond the solid solution limit would cause the precipitation of Cu-rich phase at grain boundaries. Therefore, with the increase of Cu content, the interplanar spacing of the strong diffraction peak gradually increases and tends to be stable or even slightly decreases after the Cu content reaches 1.5 wt %. All in all, the rapid solidification technique (30 m/s) can effectively suppress the formation of ordered phases B2 and DO3, and the addition of Cu can improve the crystal structure by increasing the interplanar spacing and unit cell volume.

Thermogravimetric and differential scanning calorimetric analyses (TG-DSC) were performed on Fe-6.5 wt % Si steel strips to determine their phase transformation behavior and heat stability. The TG-DSC curves of steel strip samples with different Cu contents during the nonisothermal heating procedure are shown in Figure 5. The TG curve showed that the weight of the steel strip samples altered dramatically during the nonisothermal heating process, as illustrated in Figure 5a. The samples with Cu dosage of 1.5 wt % maintained good thermal stability relative to samples with other Cu contents. It can be seen in Figure 5b that the DSC curves of different Cu dosage exhibit two distinct features, namely the ordered transition from disordered A2 phase to ordered B2+DO_3 phase and the ordered-disordered transition.[32] The Cu-added high-silicon steel strip prepared by rapid solidification technology was disordered in the initial stage of heating. Due to the high cooling rate of the solidification process, it is obvious that the samples are mainly disordered in the initial state of heating, with exothermic reactions occurring at 365−405 °C. The observed peak of the DSC curve in this temperature range was due to the transition of A2 to B2+DO_3, possibly accompanied by a partial transition of DO_3 to B2. The sample's second exothermic transition occurs at 820−865 °C, which is mostly due to the material's transition from B2 to A2. According to the DSC curve, it can be determined that both the transitions from order to disorder and from disorder to order are exothermic transition.

3.3. Microstructure and Energy Spectrum Analysis. During rapid solidification, the high-temperature molten alloy impacts the high-speed rotating copper roller. The steel strip is forced to cool rapidly under the restraint of high-pressure Ar-fluid and copper roll. Rapid cooling technology diminishes the critical nucleation radius of the alloy and reduces the ion migration rate. The high solidification rate and undercooling

https://doi.org/10.1021/acsomega.2c07510
ACS Omega 2023, 8, 8461−8472

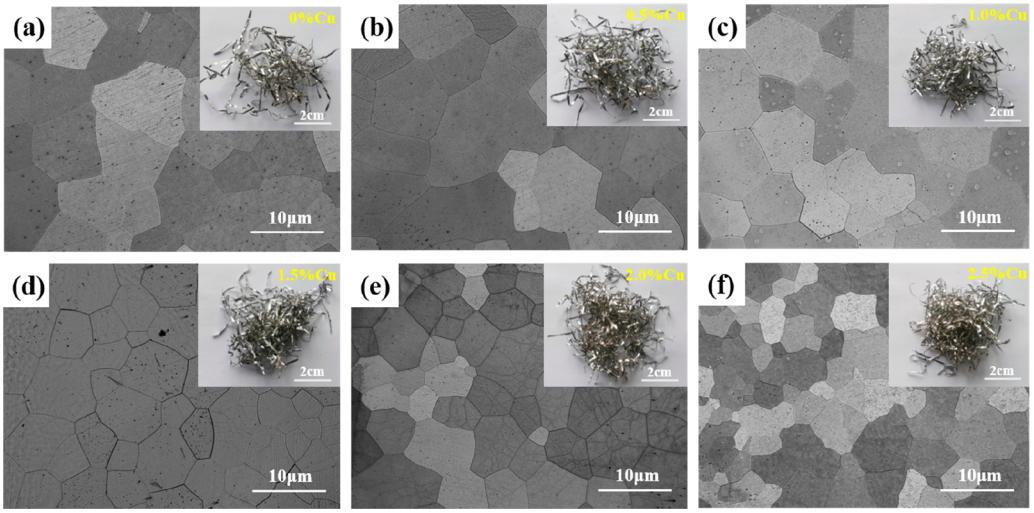

Figure 6. Metallographic structure of Fe-6.5 wt % Si steel strip with 0−2.5 wt % Cu dosage at 30 m/s: (a) 0 wt %, (b) 0.5 wt %, (c) 1.0 wt %, (d) 1.5 wt %, (e) 2.0 wt %, and (f) 2.5 wt %.

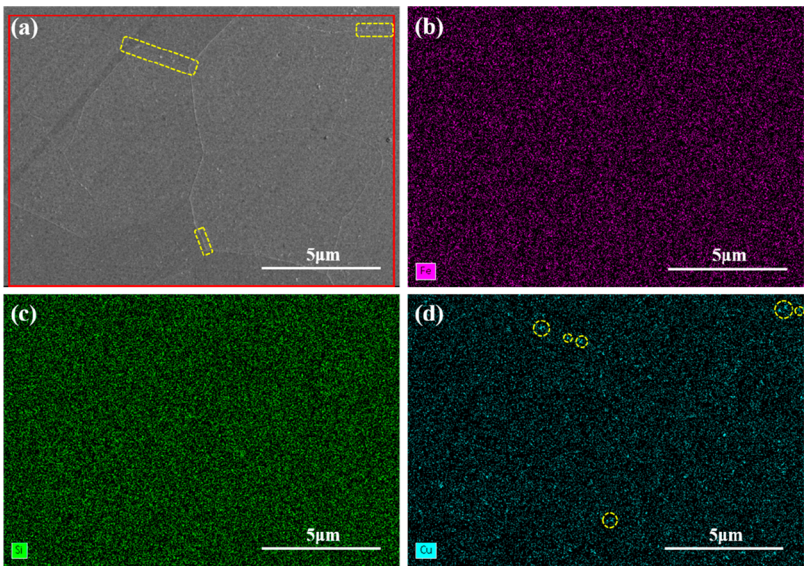

Figure 7. Microstructure and EDS maps of Fe-6.5 wt % Si steel strip with 1.5 wt % Cu dosage: (a) SEM image, (b) Fe element, (c) Si element, and (d) Cu element.

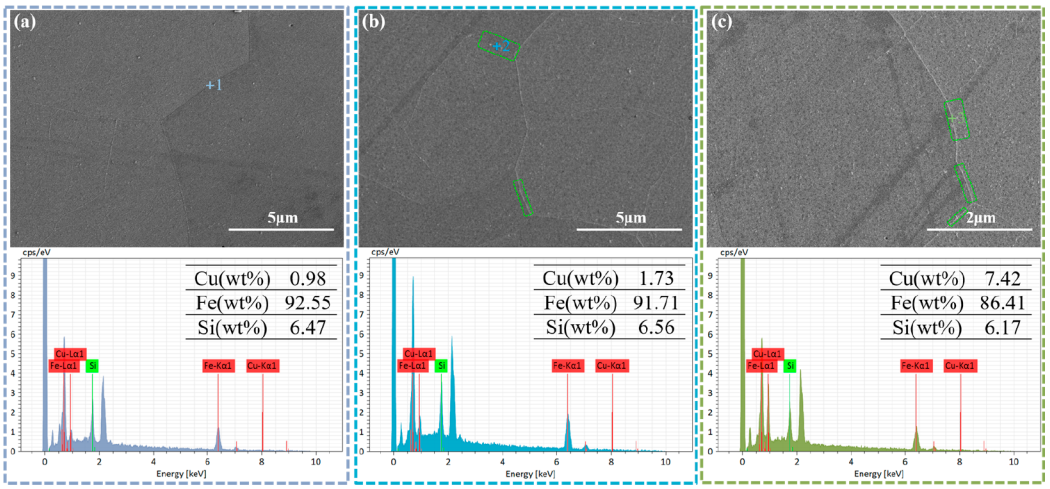

Figure 8. EDS analysis at the grain boundaries of Fe-6.5 wt % Si steel strip samples: (a) 1.0 wt % Cu, (b) 1.5 wt % Cu, and (c) 2.0 wt % Cu.

https://doi.org/10.1021/acsomega.2c07510
ACS Omega 2023, 8, 8461−8472

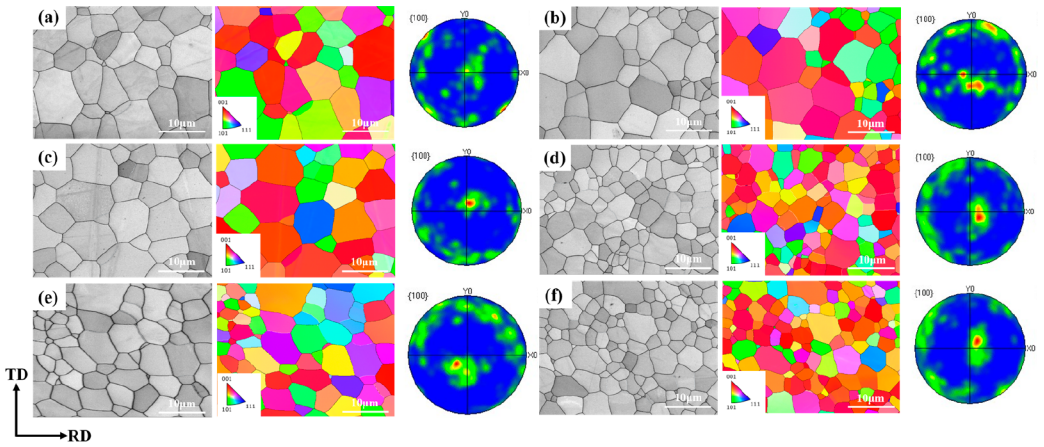

Figure 9. Microstructure, EBSD IPF Z color map, and Pole figure from the free side of the 30 m/s steel strip sample surface: (a) 0 wt % Cu, (b) 0.5 wt % Cu, (c) 1.0 wt % Cu, (d) 1.5 wt % Cu, (e) 2.0 wt % Cu, and (f) 2.5 wt % Cu.

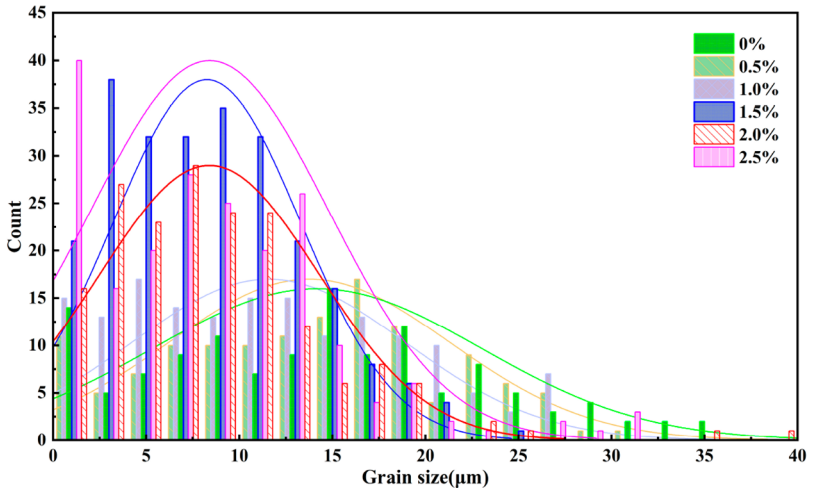

Figure 10. Grain size distribution of Fe-6.5 wt % Si steel strip with 0−2.5 wt % Cu dosage.

make the alloy nucleate rapidly and increase the solid solution limit.

As shown in the surface micrographs of Figures 6, the Cu-added high-silicon steel strip at the cooling rate of 30 m/s all exhibit equiaxed fine grains. It can also be clearly seen that the average grain size decreases with the addition of Cu. However, with the further increase of Cu dosage, the tendency of grain size to become smaller becomes weaker. The grain refinement phenomenon after adding Cu may be because the high-silicon steel will nucleate with nano-Cu particles, thus forming a large number of equiaxed fine grains. However, when the dosage of Cu exceeds 1.5 wt %, Cu particles will be enriched at the grain boundary to form Cu precipitation, which will weaken the effect of Cu grain refinement. The average grain size of Fe-6.5 wt % Si steel strip in at was 8.7 μm, showing regular central equiaxed fine grains.

Figure 7 shows the SEM image of the Fe-6.5 wt % Si steel strip with 1.5 wt % Cu and the corresponding EDS spatial elemental mapping of the steel strip. The microstructure of the rapidly solidified steel strip samples consisted of uniform equiaxed grains (Figure 7). The addition of Cu makes the microstructure of Fe-6.5 wt % Si steel strip slightly refined, and when the dosage of Cu reaches 1.5 wt %, Cu-rich precipitates[18] appear at the grain boundaries, as shown in Figure 7a. Figure 7b,c shows that Fe and Si elements are uniformly distributed at the grain boundaries and inside the grains, indicating that repeated smelting makes the element distribution with high consistency. As shown in Figure 7d, the Cu element appears to have a small amount of aggregation at the grain boundaries, confirming the appearance of Cu-rich precipitates at the grain boundaries.

Further SEM microstructural examination revealed that Cu-rich precipitates were absent in the 1.0 wt % Cu specimen (Figure 8a), but became visible in the 1.5 wt % Cu specimen (Figure 8b). The precipitates in the 1.5 wt % Cu specimen were tiny, few, and irregularly scattered at grain boundaries. Cu-rich precipitates were continuous or semicontinuous at grain boundaries as the Cu dosage was raised to 2.0 wt %, as shown in Figure 8c. As demonstrated in Figure 14, the accumulation of these Cu-rich precipitates embrittles the grain boundaries and cause poor flexibility of the steel strip, thereby affecting the mechanical properties. Therefore, it can be concluded that when the dosage of Cu is >1.0 wt %, the plasticity of the steel strip is reduced due to the limited solubility of Cu in the steel strip, and the Cu-rich precipitates are precipitated at the grain boundaries. The absence of such precipitates in the 1.0 wt % Cu steel strip indicates that the solubility of Cu in the steel strip prepared by the rapid solidification technique is less than or near to 1.5 wt %.

https://doi.org/10.1021/acsomega.2c07510
ACS Omega 2023, 8, 8461−8472

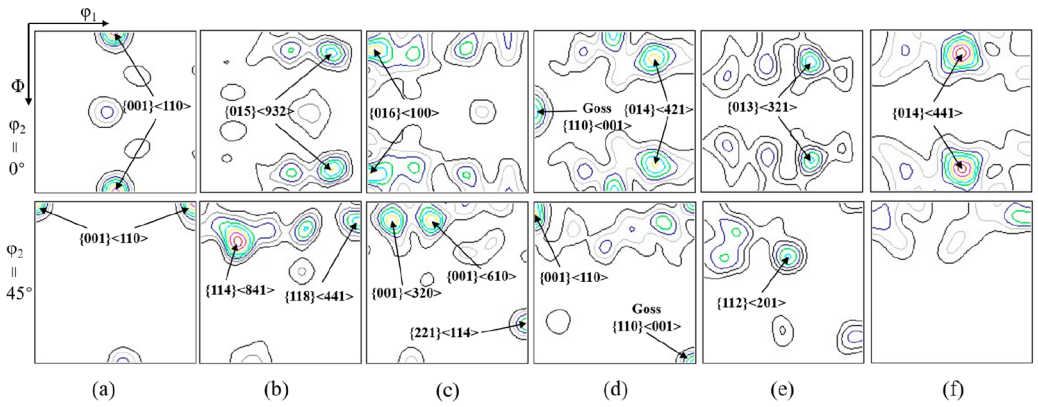

Figure 11. ODF sections of φ_2 = 0° and 45° of specimens with different contents of Cu added: (a) 0 wt % Cu, (b) 0.5 wt % Cu, (c) 1.0 wt % Cu, (d) 1.5 wt % Cu, (e) 2.0 wt % Cu, and (f) 2.5 wt % Cu (grade: 1, 2, 3, 4, 5, 6, 7, 8, 9, 10, ...).

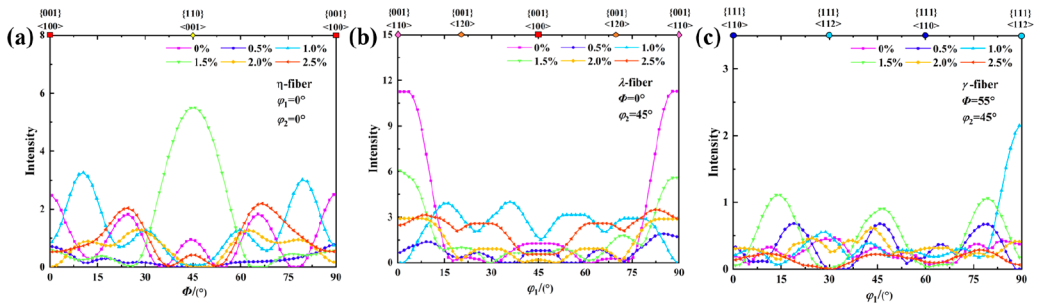

Figure 12. Orientation line density map for η, λ, and γ textures: (a) η-fibers, (b) λ-fibers, and (c) γ-fibers.

3.4. Texture Evolution Mechanism. The high permeability and high saturation magnetic induction of high silicon steel reduce the dependence of its magnetic properties on crystal orientation to a certain extent. However, according to actual production requirements, the magnetic properties of high silicon steel can still be improved through texture control and optimization.

Figure 9 shows the EBSD microstructure, orientation diagram, and the corresponding pole figure of the steel strip. In order to more intuitively reflect the change of average grain size, the normal distribution function of grain size of steel strips with different Cu dosage is drawn, as shown in Figure 10. It can be clearly seen that the grain size of steel strip gradually becomes smaller with the increase of Cu dosage, and the average grain size tends to stabilize after Cu dosage reaches 1.5 wt %. The average grain size of the 1.5 wt % Cu steel strip samples is 8.7 μm. As shown in Figure 9 (EBSD IPF map), the Cu-added steel strip sample had a strong ⟨100⟩ fiber texture. From the pole figure, it can be measured that the deviation from the normal direction of the plate is about 20°. The steel strip sample without Cu had no obvious preferred orientation, and the average grain size was 14.3 μm as shown in Figure 9a, and according to the microstructure (Figure 10) measured by EBSD, the grains of the 1.5 wt % Cu sample were more uniform small with good consistency.

Figure 11 illustrates the deformed texture of the steel strip sample. The sample with 0 wt % Cu dosage shows a strong single λ-fiber texture with a peak near {001}⟨110⟩. With the addition of Cu, the λ-fiber texture gradually disappeared, and the 0.5 wt % Cu steel strip appeared α*-fiber texture with a peak around {114}⟨841⟩, and with the increase of Cu content, the α-fiber texture represented by {016}⟨100⟩ appeared in the steel strip samples to replace the α*-fiber texture. The λ-fiber texture ({001}⟨110⟩) and Goss texture ({110}⟨001⟩) appeared when the Cu content increased to 1.5 wt %. In the 2.0 wt % Cu and 2.5 wt % Cu steel strip samples, there is no obvious preferred orientation, and the λ-fiber texture and Goss texture disappear. It should be noted that the Goss texture had appeared in the 1.5 wt % Cu steel strip, and the relative strength of the texture reaches 5.51.

The optimization control of high silicon steel texture is divided into two directions: strong λ-fibers texture control and strong η-fibers texture control system. The λ-fiber texture (⟨001⟩//ND) is characterized by two ⟨001⟩ orientations on the rolling surface, which is easy to magnetize and has a high magnetic induction.[33,34] The η-fibers texture is ⟨100⟩//RD, which is characterized in that the rolling direction is in the most easily magnetization direction, and higher magnetic induction and lower iron loss can be obtained by rolling upward. However, the magnetic anisotropy of the material is obvious, and the rolling magnetism is quite different from the transverse magnetism.

In order to intuitively reflect the influence of Cu on η, λ and γ texture, according to the Typical texture components of electrical steel (Figure 2), Figure 12 shows the orientation line density diagram of η, λ, and γ texture. The intensity of η-fibers texture (⟨001⟩//RD) first increases and then decreases with the increase of Cu, as shown in Figure 12a. The η-fibers texture represented by the Goss texture ({110}⟨001⟩) appeared when the Cu dosage was 1.5 wt %. Although the strength of the λ-fibers texture ({001}//ND) is slightly reduced after the addition of Cu, the 1.5 wt % Cu steel strip still has a certain strength of the λ-fibers texture ({001}⟨100⟩), as shown in Figure 12b. As shown in Figure 12c, all the steel strip samples do not have γ-fibers texture, which is detrimental to the magnetic properties.[35−37]

https://doi.org/10.1021/acsomega.2c07510
ACS Omega 2023, 8, 8461−8472

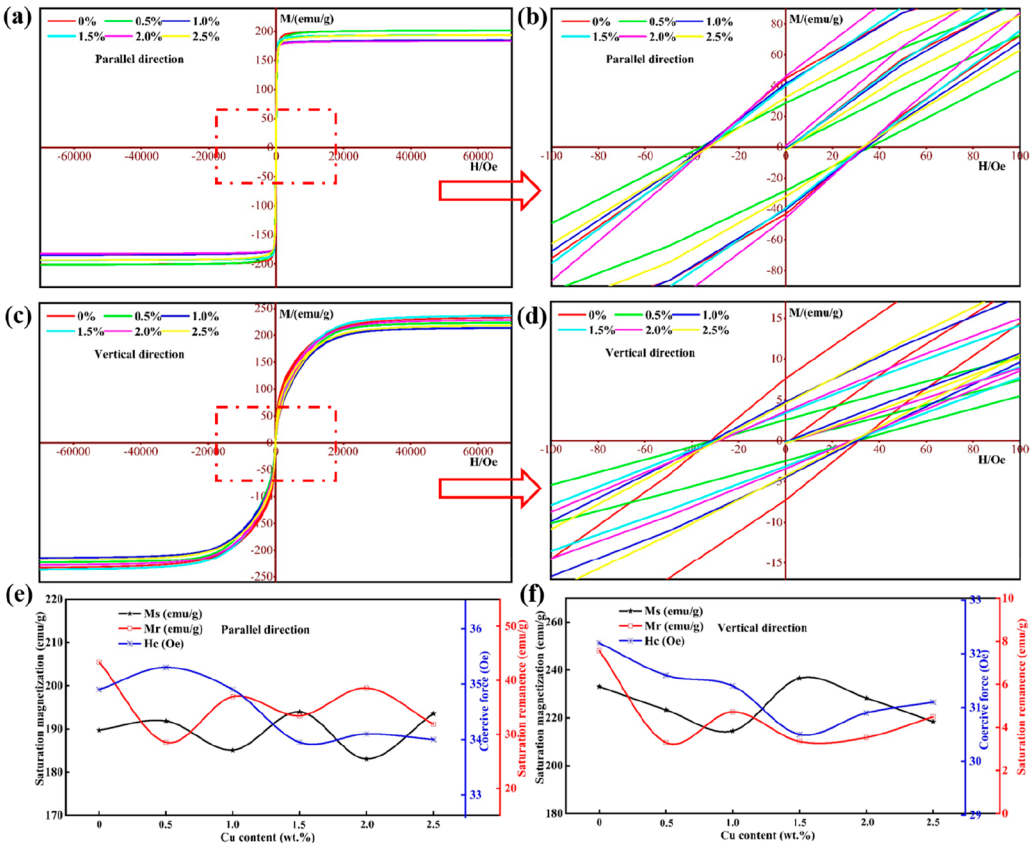

Figure 13. (a,b) Hysteresis loops at room temperature of Fe-6.5 wt % Si samples with 0−2.5 wt % Cu dosage at the parallel direction. (c,d) Hysteresis loops at room temperature of Fe-6.5 wt % Si samples with 0−2.5 wt % Cu dosage at the vertical direction. (e) Magnetic properties of the Fe-6.5 wt % Si samples at the parallel direction. (f) Magnetic properties of the Fe-6.5 wt % Si samples at the vertical direction.

In conclusion, after adding Cu, the original λ-fibers texture is still retained and the η-fibers texture appears. The Cu-added high-silicon steel strip is composed of η-fibers texture, λ-fibers texture, and a small amount of γ-fibers texture. It should be noted that the 1.5 wt % Cu steel strip samples consist of significant η-fibers texture, λ-fibers texture, and Goss texture.

3.5. Magnetic and Mechanical Properties. The magnetic properties of the steel strip samples with Cu dosages of 0−2.5 wt % were measured by the vibrating sample magnetometer at room temperature. The hysteresis loops exhibit that the steel strip specimen is a typical crystalline soft magnetic material, as shown in Figure 13a−d. In order to intuitively express the effect of Cu dosage on the magnetic properties of the steel strip, the saturation magnetization (M_s), coercive force (H_c) and saturation remanence (M_r) were calculated from the data of Figure 13a−d, as shown in Figure 13e,f. The magnetic anisotropy of the steel strip samples is obvious, and the magnetic hysteresis loops in the direction parallel to the vertical plate surface are obviously different.[38,39] The anisotropy of the hysteresis loops is mainly attributed to the η-fibers texture ($\langle 001 \rangle$//RD) of the steel strip samples, as shown in Figure 12. The η-fibers texture will increase the magnetic anisotropy while improving the magnetic properties of the material.

Figure 13a,e confirms that the M_s does not change significantly when the magnetic properties of the steel strip sample are measured parallel to the direction of the external magnetic field (0 °C). The M_r of the steel strip samples decreased slightly after adding Cu (Figure 13b,e). The H_c decreases gradually before the Cu dosage was 1.5 wt %, and increasing the Cu dosage from 1.5 wt % to 2.5 wt % had no significant effect. In contrast, the magnetic properties of the 1.5 wt % Cu steel strip samples are relatively good, with M_s, M_r, and H_c values of 193.94 emu/g, 33.45 emu/g, and 33.95 Oe, respectively. Figure 13c,d,f is the magnetic properties of the steel strip samples measured perpendicular to the direction of the external magnetic field (90 °C). The hysteresis loop shows that the magnetization behavior fluctuates obviously, which is probably due to the grain growth orientation and the preferred orientation of the texture. In contrast, the magnetic properties of the 1.5 wt % Cu steel strip sample also performed the best, with M_s, M_r, and H_c of 236.54 emu/g, 3.34 emu/g, and 30.52 Oe.

As shown in Figure 13e,f, when measuring the magnetic properties of the steel strip samples, compared with the external magnetic field (90 °C) perpendicular to the external magnetic field (0 °C), M_s increased significantly (193.94 emu/g to 236.54 emu/g), M_r decreased significantly (33.45 emu/g to 3.34 emu/g), and H_c remained basically unchanged (33.95 to 30.52 Oe). By comprehensive analysis of the crystal parameters (Figure 4c,d), the texture evolution (Figures 11 and 12), and the magnetic property curves (Figure 13), large interplanar spacing, good crystallinity, ultrafine grain distribution, and favorable texture composition can promote electron movement and thus improve magnetization efficiency. In the magnetization process, grain refinement can improve the rotation of the magnetic domain, and promote the migration of the magnetic domain wall to refinement the magnetic domain, thereby reducing the hysteresis loss.[26] When the Cu dosage was increased beyond 1.5 wt %, the precipitation of Cu-rich

https://doi.org/10.1021/acsomega.2c07510
ACS Omega 2023, 8, 8461−8472

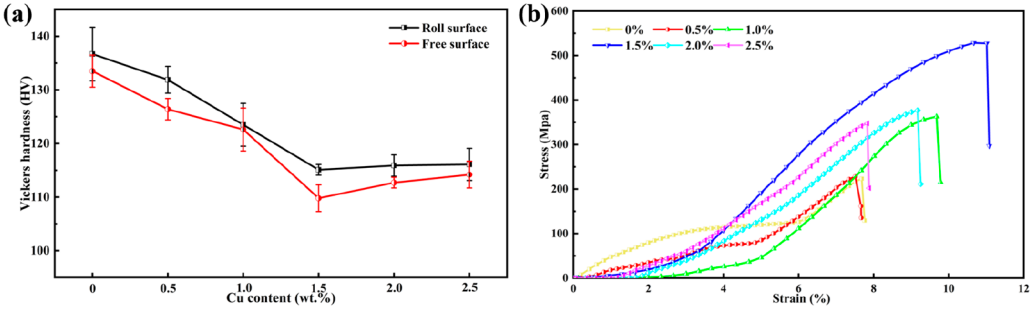

Figure 14. (a) Vickers hardness and (b) engineering stress−strain curves of the Fe-6.5 wt % Si steel strip with 0−2.5 wt % Cu dosage.

particles at grain boundaries will hinder the movement of electrons and the rotation of magnetic domains, thus worsening the magnetic properties, and the η-fibers texture and λ-fibers textures can effectively improve the magnetic properties of high silicon steel strip. In conclusion, it is precisely because the 1.5 wt % Cu steel strip sample is composed of significant η-fiber texture, λ-fiber texture, and Goss texture. The steel strip with the dosage of 1.5 wt % Cu has the best M_r property and appropriate M_s and H_c properties.

Figure 14a exhibits the Vickers hardness curves of Fe-6.5 wt % Si steel strips with Cu dosage ranging from 0 wt % to 2.5 wt %. The Vickers hardness of steel strip declines progressively as Cu dosage increases, becoming steady after 1.5 wt %, and the hardness of the roll surface is always larger than that of the free surface. The difference in Vickers hardness between the roll surface and the free surface is mainly owing to the varying degrees of solidification rates and contact media (roll and airflow) on both sides of the strip.[40] The roll surface has a slightly higher Vickers hardness than the free surface, owing to the fact that the roll surface is restricted by the copper roll during the solidification process, making the roll surface's grains more compact and regular. Moreover, the decrease of Vickers hardness of Fe-6.5 wt % Si steel strip is obviously correlated with the decrease of grain size, as shown in Figure 6. The hardness of Vickers decreases with the decrease of grain size. The decrease of grain size is mainly due to the introduction of nano-Cu precipitate which hinders the migration and growth of grain boundaries during solidification. At the same time, the nano-Cu precipitate will make the grain boundary unstable and facilitate the generation of total dislocation,[17,33,38] thus promoting the softening behavior and reducing the Vickers hardness. Through the rapid solidification technique, the ordered phases (B2 and DO_3) are effectively inhibited, improving sample ductility. The engineering stress−strain curves of the steel strip samples are shown in Figure 14b. With the increase of Cu dosage, the plasticity of the steel strip increases gradually until 1.5 wt %. When the Cu dosage is between 1.5 wt % and 2.5 wt %, the plasticity of the steel strip decreases slightly.

The dissolution of Cu in the solid solution reduces the long-range order of Fe-6.5Si (wt %) alloys, thereby improving the ductility of the alloys. The dosage of Cu exceeds the solid solution limit, which leads to the precipitation of Cu-rich phase at the grain boundary,[17,18] which embrittles the grain boundary, thereby seriously reducing the plasticity of the alloy. Therefore, the mechanical properties of Fe-6.5 wt % Si ribbons are greatly improved. The Vickers hardness of the roll surface and free surface of the 1.5 wt % Cu steel strip is 115.1 HV and 109.8 HV, respectively, and the 1.5 wt % Cu steel strip sample had a plastic deformation at failure of about 11%.

3.6. First-Principles Calculations. In the disordered A2 phase, Fe and Si are distributed randomly. At a rapid cooling rate of 30 m/s, the ordered phases (B2 and DO_3) of Fe-6.5 wt % Si were basically suppressed as shown in Figure 4. Therefore, a model was established to explore the effect of Cu on the disordered phase A2 of the high-silicon steel strip. A2 disordered structures of Fe-12.5 atom %Si and Fe-12 atom %Si-1 atom %Cu, as shown in Figure 15, have been considered for the study of structure stability and magnetic properties.

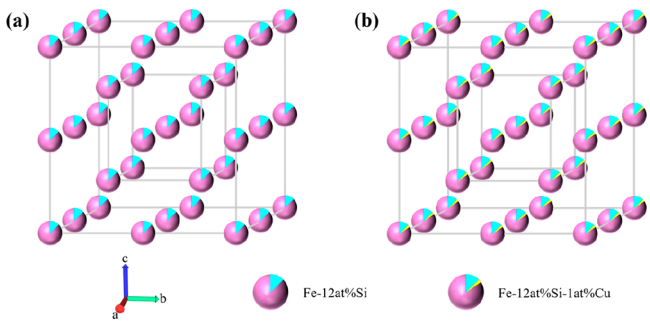

Figure 15. Crystal structures of Fe-12 atom %Si with different Cu dosage for A2 phases: (a) 0 atom %Cu and (b) 1 atom %Cu. Purple, cyan and yellow atoms are Fe, Si, and Cu, respectively.

In order to further explore the interaction between the alloy atom Cu and the other atoms in the crystal cell and study the effect of Cu on the bonding efficiency of the system, the effects of alloying element Cu on the density of states (TDOS)[41] and fractional density of states (PDOS)[42] of Fe-12 atom % Si were calculated, as shown in Figure 16. Figure 16a shows the calculated density of states of Fe-12.5 atom %Si, the dotted line in the figure represents the position of the Fermi level (E^F), and Figure 16b shows the density of states (DOS) of each alloy in Fe-12 atom % Si-1 atom % Cu. From the DOS diagram of the Fe-12 atom % Si-1 atom % Cu alloy in Figure 16b, it can be seen that the bonding electrons are mainly distributed in two intervals of −4.2 to −5.1 eV and −5.3 to −5.9 eV. The Fe 3d, Cu 3d, and Si 2p orbitals have obvious bonding peaks near the Fermi level in the PDOS diagram. The hybridization of these three orbitals results in sharp resonance peaks near the Fermi level in the density of states diagram. The hybridization of these three orbitals causes a sharp formant near the Fermi level of the density diagram, indicating that Fe, Cu, and Si bond here. Although Si atoms provide bonding electrons in the range of −5.3 to −5.9 eV, the density of Fe and Cu states in this range is almost zero. Therefore, in Fe-12 atom % Si-1 atom % Cu alloys, Fe 3d, Cu 3d, and Si 2p orbitals provide bonding electrons and are the main factors for bonding.

https://doi.org/10.1021/acsomega.2c07510
ACS Omega 2023, 8, 8461−8472

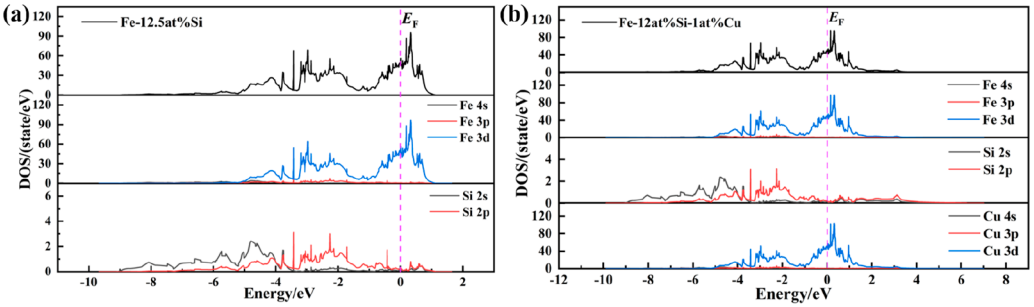

Figure 16. DOS of Fe-12 atom %Si with different Cu dosage for A2 phases: (a) 0 atom %Cu and (b) 1 atom %Cu.

After examining the phase combination before and after Cu addition, the relative stability, total magnetic moment,[1] and magnetic moment contribution[43] of Cu of these phases are shown in Table 1. The comparison of binding energies before and after Cu addition shows that the A2 disordered phase with 1 atom % Cu is more stable. And the A2 disordered phase with Fe-12 atom % Si-1 atom % Cu has a higher magnetic moment of 27.6454 μ_B. The increase in magnetic moment in the A2 disordered phase supports our observation of higher M_s in the 1.5 wt % Cu high silicon steel strip sample (Figure 13). The magnetic moment contribution of Cu in Fe-12 atom % Si-1 atom % Cu is 2.16 μ_B. In the meantime, we also calculated that the total magnetic moment of the A2 disordered phase with Fe-6.5 atom %Si composition is 29.6184 μ_B, which is significantly higher than that of Fe-12 atom %Si composition. This clearly shows that the total magnetic moment of the A2 disordered phase of silicon steel decreases with increasing Si content. The magnetic parameters calculated by the model simulation are consistent with the experimental results.

Table 1. Energy, Binding Energy, Magnetic Moment of Fe−Si−Cu and Magnetic Moment of Cu under Different Doping Configurations

Doping density	Binding energy (eV/atom)	Total magnetic moment (μ_B)	Magnetic moment of Cu (μ_B)
0 atom %	−53.346122	26.5178	0
1 atom %	−92.6186421	27.6454	2.16

4. CONCLUSION

The ordered phases (B2, DO_3) of the high-silicon steel strip prepared in the rapid solidification technique were effectively suppressed. On this basis, Cu-dosage could significantly improve the strip length, plasticity, and magnetic property. The high silicon strip length increases by 200% with 1.5 wt % Cu dosage. The average grain size and Vickers hardness decrease with the increase of Cu dosage, which is mainly due to the Cu-rich particles precipitating at the grain boundary, nailing the grain boundaries movement, and inhibiting the grain growth. The plasticity increases first before 1.5 wt % Cu-dosage and then decreases, which is attributed to the aggregation of Cu elements at grain boundaries to form Cu-rich precipitates. Cu-dosage promotes the formation of the η-fiber structure and inherits the λ-fiber structure, while the Goss texture ($\{110\}\langle001\rangle$) forms with 1.5 wt % Cu-dosage. Cu-dosage optimizes the texture and improves the magnetic properties of high-silicon steel strip, and the M_s, M_r, and H_c of the 1.5 wt % Cu sample in the perpendicular magnetization direction are 236.54 emu/g, 3.34 emu/g, and 30.52 Oe. The experimental and theoretical modeling results indicate that Cu could enhance the magnetic properties of high-silicon steel strips.

AUTHOR INFORMATION

Corresponding Authors

Bo Wang − *Hebei Key Laboratory of Material Near-net Forming Technology, School of Materials Science and Engineering, Hebei University of Science and Technology, Hebei 050018, China;* orcid.org/0000-0002-0466-6323; Email: wangbo1996@gmail.com

Cheng Ma − *Technology Research Institute, HBIS Group, Hebei 052160, China;* Email: macheng01@hbisco.com

Authors

Di Zhang − *Hebei Key Laboratory of Material Near-net Forming Technology, School of Materials Science and Engineering, Hebei University of Science and Technology, Hebei 050018, China;* orcid.org/0000-0001-9113-7050

Yingtao Su − *Hebei Key Laboratory of Material Near-net Forming Technology, School of Materials Science and Engineering, Hebei University of Science and Technology, Hebei 050018, China*

Xingrui Yang − *Hebei Key Laboratory of Material Near-net Forming Technology, School of Materials Science and Engineering, Hebei University of Science and Technology, Hebei 050018, China*

Huilan Sun − *Hebei Key Laboratory of Material Near-net Forming Technology, School of Materials Science and Engineering, Hebei University of Science and Technology, Hebei 050018, China*

Zhihong Guo − *Hebei Key Laboratory of Material Near-net Forming Technology, School of Materials Science and Engineering, Hebei University of Science and Technology, Hebei 050018, China*

Zhongqi Dong − *Hebei College of Industry and Technology, Hebei 050091, China*

Liguang Zhu − *Hebei Key Laboratory of Material Near-net Forming Technology, School of Materials Science and Engineering, Hebei University of Science and Technology, Hebei 050018, China*

Complete contact information is available at: https://pubs.acs.org/10.1021/acsomega.2c07510

Notes

The authors declare no competing financial interest.

ACKNOWLEDGMENTS

This work was supported by the National Natural Science Foundation of China (51974103, 51974102), the Natural

https://doi.org/10.1021/acsomega.2c07510
ACS Omega 2023, 8, 8461−8472

Science Foundation of Hebei Province (E2019208308, E2022208068), Key Research and Development Program of Hebei Province (20311005D).

REFERENCES

(1) Ouyang, G.; Macziewski, C. R.; Jensen, B.; Ma, T.; Choudhary, R.; Dennis, K.; Zhou, L.; Paudyal, D.; Anderson, I.; Kramer, M. J.; Cui, J. Effects of Solidification Cooling Rates on Microstructures and Physical Properties of Fe-6.5%Si Alloys. *Acta Mater.* **2021**, *205*, 116575.
(2) Liang, Y. F.; Ye, F.; Lin, J. P.; Wang, Y. L.; Chen, G. L. Effect of Annealing Temperature on Magnetic Properties of Cold Rolled High Silicon Steel Thin Sheet. *J. Alloys Compd.* **2010**, *491*, 268−270.
(3) Zheng, Z. L.; Ye, F.; Liang, Y. F.; Ding, X. F.; Lin, J. P.; Chen, G. L. Formation of Columnar-Grained Structures in Directionally Solidified Fe-6.5wt.%Si Alloy. *Intermetallics* **2011**, *19*, 165−168.
(4) Lin, G.; Zhao, F.; Yu, X.; Zhang, Z.; Xie, J. Effect of Annealing on Microstructure, Texture and Magnetic Properties of Fe-6.5 wt%Si-0.03 wt%Nb Alloy. *J. Magn. Magn. Mater.* **2020**, *504*, 166699.
(5) Tang, W.; Ouyang, G.; Cui, B.; Wang, J.; Dennis, K. W.; Kramer, M. J.; Anderson, I. E.; Cui, J. Magnetic and Mechanical Properties of Grain-Refined Dy-Free Nd-Fe-B Sintered Magnets. *J. Magn. Magn. Mater.* **2021**, *521*, 167533.
(6) Ouyang, G.; Chen, X.; Liang, Y.; Macziewski, C.; Cui, J. Review of Fe-6.5 wt%Si High Silicon Steel—A Promising Soft Magnetic Material for Sub-kHz Application. *J. Magn. Magn. Mater.* **2019**, *481*, 234−250.
(7) Cui, S.; Ouyang, G.; Ma, T.; Macziewski, C. R.; Levitas, V. I.; Zhou, L.; Kramer, M. J.; Cui, J. Thermodynamic and Kinetic Analysis of the Melt Spinning Process of Fe-6.5 wt.% Si Alloy. *J. Alloys Compd.* **2019**, *771*, 643−648.
(8) Cai, G.; Wang, Y.; Huang, Y.; Misra, R. D. K. Ordered Structure, Dislocation, and Grain Boundary Character Distribution and Their Effects on Warm Deformation in Soft-Magnetic Fe−6.9Si−0.01B Alloy. *Steel Res. Int.* **2021**, *92*, 2000269.
(9) Li, C. S.; Yang, C. L.; Cai, G. J.; Wang, Q. W. Ordered Phases and Microhardness of Fe-6.5%Si Steel Sheet after Hot Rolling and Annealing. *Mater. Sci. Eng., A* **2016**, *650*, 84−92.
(10) Cava, R. D.; Botta, W. J.; Kiminami, C. S.; Olzon-Dionysio, M.; Souza, S. D.; Jorge, A. M.; Bolfarini, C. Ordered Phases and Texture in Spray-Formed Fe-5 wt%Si. *J. Alloys Compd.* **2011**, *509*, S260−S264.
(11) Wang, Z. J.; Li, Y. W.; Wang, G. D.; Liu, H. T. Effects of Boron Content on the Microstructure and Mechanical Properties of Twin-Roll Strip Casting Borated Steel Sheets. *Mater. Sci. Eng., A* **2020**, *793*, 139847.
(12) Wang, B.; Li, G.; Wang, Y.; Su, Y.; Sun, H.; Guo, Z.; Zhang, D.; Dong, Z. Characterization of the Fe-6.5 wt %Si Strip with Rapid Cooling Coupling Deep Supercooled Solidification. *ACS Omega* **2021**, *6*, 25412−25420.
(13) Luo, Z.; Fan, X.; Hu, W.; Luo, F.; Li, G.; Li, Y.; Liu, X.; Wang, J. Controllable SiO2 Insulating Layer and Magnetic Properties for Intergranular Insulating Fe-6.5wt.%Si/SiO2 Composites. *Adv. Powder Technol.* **2019**, *30*, 538−543.
(14) Fan, X. A.; Wu, Z. Y.; Li, G. Q.; Wang, J.; Xiang, Z. D.; Gan, Z. H. High Resistivity and Low Core Loss of Intergranular Insulated Fe-6.5 wt.%Si/SiO2 Composite Compacts. *Mater. Des.* **2016**, *89*, 1251−1258.
(15) Liu, H. T.; Li, H. Z.; Li, H. L.; Gao, F.; Liu, G. H.; Luo, Z. H.; Zhang, F. Q.; Chen, S. L.; Cao, G. M.; Liu, Z. Y.; Wang, G. D. Effects of Rolling Temperature on Microstructure, Texture, Formability and Magnetic Properties in Strip Casting Fe-6.5 wt% Si Non-Oriented Electrical Steel. *J. Magn. Magn. Mater.* **2015**, *391*, 65−74.
(16) Han, C.; Wen, S.; Ye, F.; Wu, W.; Xue, S.; Liang, Y.; Liu, B.; Lin, J. Deformation Twinning in Equiaxed-Grained Fe-6.5 wt.%Si Alloy after Rotary Swaging. *J. Mater. Sci. Technol.* **2020**, *49*, 25−34.
(17) Gao, J.; Jiang, S.; Zhang, H.; Huang, Y.; Guan, D.; Xu, Y.; Guan, S.; Bendersky, L. A.; Davydov, A. V.; Wu, Y.; Zhu, H.; Wang, Y.; Lu, Z.; Rainforth, W. M. Facile Route to Bulk Ultrafine-Grain Steels for High Strength and Ductility. *Nature* **2021**, *590*, 262−267.
(18) Cheng, Z. Y.; Liu, J.; Xiang, Z. D.; Jia, J.; Bi, Y. J. Effects of Cu Addition on Plasticity of Fe-6.5Si (wt.%) Alloy at Temperatures below 550 °C. *Intermetallics* **2020**, *120*, 106747.
(19) Lamichhane, T. N.; Sethuraman, L.; Dalagan, A.; Wang, H.; Keller, J.; Paranthaman, M. P. Additive Manufacturing of Soft Magnets for Electrical Machines—a Review. *Mater. Today Phys.* **2020**, *15*, 100255.
(20) Feng, Y.; Li, Y.; Guo, J.; Li, J.; Du, T. Effect of Slab Reheating Temperature on Recrystallization Microstructure, Texture and Magnetic Properties of Nb-Containing Grain-Oriented Silicon Steel. *J. Magn. Magn. Mater.* **2017**, *439*, 135−143.
(21) Cai, G.; Li, C.; Cai, B.; Wang, Q. An Investigation on the Role of Texture Evolution and Ordered Phase Transition in Soft Magnetic Properties of Fe−6.5 wt%Si Electrical Steel. *J. Magn. Magn. Mater.* **2017**, *430*, 70−77.
(22) Zhang, D.; Su, Y.; Li, G.; Guo, Z.; Sun, H.; Wang, B.; Zhu, L. Grain Boundary Diffusion Effect on Mineral Transition of Calcium Sulpho-Aluminate with Sodium Dopant. *Ceram. Int.* **2021**, *47*, 20923−20934.
(23) Liu, D.; Qin, J.; Zhang, Y.; Wang, Z.; Nie, J. Effect of Yttrium Addition on the Hot Deformation Behavior of Fe−6.5 wt%Si Alloy. *Mater. Sci. Eng., A* **2020**, *797*, 140238.
(24) Cai, G.; Yang, Y.; Huang, Y.; Misra, R. D. K. The Significance of Ce on Hot Compression Deformation and Mechanical Behavior of Fe−6.9 wt%Si Alloy: Decrease of Order Degree and Transformation of Dislocations. *Mater. Charact.* **2020**, *163*, 110220.
(25) Cheng, Z.; Liu, J.; Xiang, Z.; Jia, J.; Volkova, O.; Wendler, M. Effect of Cu Addition on Microstructure, Texture and Magnetic Properties of 6.5 wt% Si Electrical Steel. *J. Magn. Magn. Mater.* **2021**, *519*, 167471.
(26) Ouyang, G.; Jensen, B.; Macziewski, C. R.; Ma, T.; Meng, F.; Lin, Q.; Zhou, L.; Kramer, M.; Cui, J. Characterization of Ordering in Fe-6.5%Si Alloy Using X-Ray, TEM, and Magnetic TGA Methods. *Mater. Charact.* **2019**, *158*, 109973.
(27) Du, Y.; Hu, X.; Zhang, S.; Song, Y.; Jiang, H.; Rong, L. Precipitation Behavior of Cu-NiAl Nanoscale Particles and Their Effect on Mechanical Properties in a High Strength Low Alloy Steel. *Mater. Charact.* **2022**, *190*, 112014.
(28) Sun, H.; Li, D.; Diao, Y.; He, Y.; Yan, L.; Pang, X.; Gao, K. Nanoscale Cu Particle Evolution and Its Impact on the Mechanical Properties and Strengthening Mechanism in Precipitation-Hardening Stainless Steel. *Mater. Charact.* **2022**, *188*, 111885.
(29) Ueshima, N.; Maeda, T.; Oikawa, K. Effect of Cu Addition on Precipitation and Growth Behavior of MnS in Silicon Steel Sheets. *Metall. Mater. Trans. A Phys. Metall. Mater. Sci.* **2017**, *48*, 3843−3851.
(30) Ouyang, G.; Jensen, B.; Tang, W.; Schlagel, J.; Hilliard, B.; Pan, C.; Cui, B.; Dennis, K.; Jiles, D.; Monson, T.; Anderson, I.; Kramer, M. J.; Cui, J. Near Net Shape Fabrication of Anisotropic Fe-6.5%Si Soft Magnetic Materials. *Acta Mater.* **2020**, *201*, 209−216.
(31) Wang, S.; Jiang, Y. M.; Liang, Y. F.; Ye, F.; Lin, J. P. Magnetic Properties and Core Loss Behavior of Fe-6.5wt.%Si Ribbons Prepared by Melt Spinning. *Adv. Mater. Sci. Eng.* **2015**, *2015*, 410830.
(32) Lemke, J. N.; Simonelli, M.; Garibaldi, M.; Ashcroft, I.; Hague, R.; Vedani, M.; Wildman, R.; Tuck, C. Calorimetric Study and Microstructure Analysis of the Order-Disorder Phase Transformation in Silicon Steel Built by SLM. *J. Alloys Compd.* **2017**, *722*, 293−301.
(33) Cheng, Z.; Liu, J.; Xiang, Z.; Jia, J.; Volkova, O.; Wendler, M. Effect of Cu Addition on Microstructure, Texture and Magnetic Properties of 6.5 wt% Si Electrical Steel. *J. Magn. Magn. Mater.* **2021**, *519*, 167471.
(34) Jiao, H.; Xu, Y.; Zhao, L.; Misra, R. D. K.; Tang, Y.; Liu, D.; Hu, Y.; Zhao, M.; Shen, M. Texture Evolution in Twin-Roll Strip Cast Non-Oriented Electrical Steel with Strong Cube and Goss Texture. *Acta Mater.* **2020**, *199*, 311−325.
(35) Fan, L.; Jia, L.; Zhu, R.; He, J. Microstructure and Texture Evolution of Medium Temperature Grain-Oriented Silicon Steel Produced by Industrialization. *Metall. Res. Technol.* **2019**, *116*, 604.

https://doi.org/10.1021/acsomega.2c07510
ACS Omega 2023, 8, 8461−8472

(36) Hou, D.; Fang, F.; Wang, Y.; Zhang, Y.; Zhang, X.; Misra, R. D. K.; Yuan, G. Nanoprecipitation Behavior and Resultant Mechanical and Magnetic Properties in Fe−Si−Ni−Al−Mn High Strength Non-Oriented Silicon Steel. *Mater. Sci. Eng., A* **2021**, *819*, 141529.
(37) Cai, G.; Li, Z.; Huang, Y. Investigation of {001} Texture Reservation and Grain Boundary Character Distribution of Fe−6.9 wt %Si Magnetic Material by Warm−Cold Rolling. *Steel Res. Int.* **2019**, *90*, 1900093.
(38) Fang, F.; Che, S.; Hou, D.; Zhang, Y.; Wang, Y.; Zhang, W.; Yuan, G.; Zhang, X.; Misra, R. D. K.; Wang, G. Thin-Gauge Non-Oriented Silicon Steel with Balanced Magnetic and Mechanical Properties Processed by Strip Casting. *Mater. Sci. Eng., A* **2022**, *831*, 142284.
(39) Luo, Z.; Fan, X.; Hu, W.; Luo, F.; Wang, J.; Wu, Z.; Liu, X.; Li, G.; Li, Y. Formation Mechanism and Enhanced Magnetic Properties of Fe−Si/Fe2SiO4 Soft Magnetic Composites Transformed from Fe-6.5 wt%Si/α-Fe2O3 Core-Shell Composites. *J. Alloys Compd.* **2020**, *817*, 152803.
(40) Liang, Y.; Wang, S.; Qi, J.; Ye, F.; Lin, J. Microstructure and Properties of Cost-Effective Fe−6.5 wt% Si Ribbons Fabricated by Melt-Spinning. *Scr. Mater.* **2019**, *163*, 107−110.
(41) Yu, X.; Lin, G.; Zhang, Z.; Xie, J. Electronic Structure Characteristics of Fe-6.5 wt%Si Alloy Doped with Rare Earth Elements and Its Effect on Mechanical Properties. *J. Alloys Compd.* **2020**, *843*, 155916.
(42) Moreno-Ramírez, L. M.; Romero-Muñiz, C.; Law, J. Y.; Franco, V.; Conde, A.; Radulov, I. A.; Maccari, F.; Skokov, K. P.; Gutfleisch, O. Tunable First Order Transition in La(Fe,Cr,Si)13 Compounds: Retaining Magnetocaloric Response despite a Magnetic Moment Reduction. *Acta Mater.* **2019**, *175*, 406−414.
(43) Han, L.; Rao, Z.; Souza Filho, I. R.; Maccari, F.; Wei, Y.; Wu, G.; Ahmadian, A.; Zhou, X.; Gutfleisch, O.; Ponge, D.; Raabe, D.; Li, Z. Ultrastrong and Ductile Soft Magnetic High-Entropy Alloys via Coherent Ordered Nanoprecipitates. *Adv. Mater.* **2021**, *33*, 2102139.

https://doi.org/10.1021/acsomega.2c07510
ACS Omega 2023, 8, 8461−8472